The non-adiabatic Peierls-Heisenberg model in finite clusters

1994 J. Phys.: Condens. Matter 6 4361

(http://iopscience.iop.org/0953-8984/6/23/016)

J. Phys.: Condens. Matter 6 (1994) 4361–4374. Printed in the UK

The non-adiabatic Peierls–Heisenberg model in finite clusters

Milton Elgueta†, Carlos Esparza‡ and Jaime Rössler§

† Escuela de Ingeniería Civil, Universidad Diego Portales, Casilla 298, Santiago, Chile
‡ Departamento de Física, Universidad de Santiago de Chile, Casilla 307, Santiago 2, Chile
§ Departamento de Física, Facultad de Ciencias, Universidad de Chile, Casilla 653, Santiago, Chile

Received 6 December 1993, in final form 28 March 1994

Abstract. The exact solution for the Peierls–Heisenberg antiferromagnetic (AF) model in a finite cluster is presented. The spin–spin coupling is retained up to second neighbours. The quantum mechanical character of the phonon variables is maintained in order to properly describe the fluctuations, which have a substantial role in one dimension. The problem of the frustrated AF state is briefly addressed. For the purpose of comparison, Born–Oppenheimer (BO) calculations are also provided. A noticeable result is the fact that the (semiclassical) BO approximation *overestimates* quantum fluctuations.

1. Introduction

The electron–phonon or spin–phonon (s–ph) interaction is usually studied using the adiabatic approximation [1–5]. Although this procedure seems suitable for high-dimensional systems, it is well known [6–12] that quantum fluctuations are important in a purely one-dimensional (1D) system. The non-adiabatic effects can reduce the Peierls distortion [7, 8, 10]. In particular, for the case of 'spinless' electrons, Hirsch and Fradklin [7, 8] have concluded that the long-range order of Peierls distortion can disappear when the ionic mass decreases below a critical value. This result is also relevant for the Peierls–Heisenberg model with first-neighbour exchange, which is fully equivalent to a 1D system of interacting spinless fermions coupled to the lattice†. Therefore, the lattice quantum fluctuations are also very important in the Peierls–Heisenberg Hamiltonian; such non-adiabatic effects can be approximately accounted for by introducing a second-neighbour (frustrating) exchange [10].

The Peierls–Heisenberg and the spin-$\frac{1}{2}$ Peierls–Hubbard models are also equivalent when the Hubbard repulsion goes to infinity; this is valid for a half-filled [14] or quarter-filled [3] band.

On the other hand, the spin-Peierls distortion (SPD) has been observed in several compounds, such as TTF–Cu–BDT [15], (2,5-DCl–DCNQI)$_2$–N(CH$_3$)$_4$ [16] and others [17, 18].

In the present paper we address the effect of quantum fluctuations in Peierls–Heisenberg systems by exactly solving four- and six-site clusters; the spin-$\frac{1}{2}$ case is considered; first- and second-neighbour spin couplings are included. We retain the interaction between spins and phonons of period two; the quantum mechanical (QM) character of these phonons is preserved. The energy levels and eigenfunctions are obtained analytically, and several physical magnitudes are evaluated. Special emphasis is given to the lifetime $\mathcal{T}$ of the distorted state; the SPD is well defined only if $\mathcal{T}$ is much larger than the phonon vibration

† This equivalence is proved via a Jordan–Wigner transformation; see for example [13].

0953-8984/94/234361+14$19.50

period. In addition, the second-neighbour spin–spin correlation is used to identify an SPD. Finally, a brief discussion of SPD in a frustrated Heisenberg lattice is given.

Another goal of the present work is to compare the exact QM results and the Born–Oppenheimer (BO) approximation; this comparison provides some surprises. Previous works [7–10] contrast the QM results with the 'adiabatic limit' $M \to \infty$, but they do not perform BO calculations. We remark that the BO method goes beyond the adiabatic limit, since it restores *a posteriori* the QM character of the lattice degrees of freedom [19].

This paper is organized as follows. In section 2 the model is introduced, and the energy spectrum and associated eigenfunctions are obtained. Also, the adiabatic approximation is presented. In section 3 numerical results are shown and discussed. Finally, in section 4 the main conclusions are summarized.

2. The model

We consider a spin-$\frac{1}{2}$ Peierls–Heisenberg ring with first-neighbour (J_1) and second-neighbour (J_2) antiferromagnetic (AF) couplings. We retain only the $k = \pi$ phonon. This choice is justified by the equivalences between the AF Heisenberg and two half-filled-band fermion Hamiltonians [13, 14]; in fact, a 1D fermion system is unstable under $2k_F$ distortions [20]; k_F is the Fermi momentum.

For a macroscopic crystal, the phonons lying in the neighbourhood of $k = \pm\pi$ are important, since they describe short-range order effects; however, in our small clusters only a few values of k are allowed. The $k = \pi$ phonon is associated with a period two SPD; such distortion only affects the distance between first-neighbour spins; thus, only the interaction J_1 is coupled to the phonon field†. The Hamiltonian is

$$H = H_{ph} + H_s + H_{s-ph} \tag{1}$$

where $H_{ph} = \omega(a^\dagger a + \frac{1}{2})$ is the phonon Hamiltonian; $a^\dagger$ creates a phonon with momentum $k = \pi$ and frequency ω. The spin contribution is

$$H_s = 2J_1 \sum_\ell S_\ell \cdot S_{\ell+1} + 2J_2 \sum_\ell{}' S_\ell \cdot S_{\ell+2} \tag{2}$$

where S_ℓ is the spin-$\frac{1}{2}$ operator on site ℓ; the prime indicates that the second sum takes into account each pair $(\ell, \ell+2)$ only once. Finally

$$H_{s-ph} = \frac{2g}{\sqrt{N}}(a + a^\dagger) \sum_\ell (-1)^\ell S_\ell \cdot S_{\ell+1} \equiv \frac{2g}{\sqrt{N}}(a + a^\dagger)\Lambda \tag{3}$$

where g is a suitable measure of the s–ph coupling, since it does not depend upon system size, N.

† Note that spins are coupled to 'longitudinal phonons' in our model. In contrast, when spins couple to other lattice vibrations, like librons [2], the dimerization may break down even in the adiabatic limit.

2.1. The spin Hamiltonian

In the case of a four-atom cluster, H_s can be recast into the form

$$H_s = (J_2 - J_1)[(S')^2 + (S'')^2 - 3] + J_1[(S)^2 - 3]$$

where $S' = S_1 + S_3$, $S'' = S_2 + S_4$ and $S = S' + S''$ is the total spin operator. We note that $\{(S)^2, (S')^2, (S'')^2, S_z\}$ are compatible operators, with associated quantum numbers $\{S, S', S'', m\}$; m is a degeneracy index. Since each individual spin has the value $s = \frac{1}{2}$, the quantum numbers S' and S'' can only attain the values $\{0, 1\}$.

On the other hand, this square-shaped cluster has the symmetry group C_{4v} (we use the nomenclature of Tinkham [21]). Therefore, the eigenfunctions of H_s belong to the irreducible representations (IR) of C_{4v}. Table 1 enumerates the five energy levels of H_s, including their degeneracy; the number of independent states is $2^4 = 16$.

Table 1. The eigenenergies of H_s, their associated quantum numbers and degeneracy.

S'	S''	S	IR	Degeneracy	Energy
0	0	0	A_1	1	$-3J_2$
0	1				
		1	E	$3 \times 2 = 6$	$-J_2$
1	0				
		0	B_1	1	$J_2 - 4J_1$
1	1	1	A_2	3	$J_2 - 2J_1$
		2	B_1	5	$J_2 + 2J_1$

According to table 1, the ground state (GS) of H_s belongs to the $S = 0$ subspace. In the $J_1 > J_2 > 0$ case, the GS belongs to the B_1 IR, while in the $J_2 > J_1 > 0$ case, the GS belongs to the A_1 IR.

The B_1 GS corresponds to two ferromagnetic interpenetrated lattices ($S' = S'' = 1$), which are coupled antiferromagnetically to each other ($S = 0$). Thus, the $[B_1, S = 0]$ IR contains second-neighbour ferromagnetic correlations (like a Neél state), $S_1 \cdot S_3 = S_2 \cdot S_4 = \frac{1}{4}$.

On the other hand, the $[A_1, S = 0]$ IR corresponds to two uncoupled singlet states, 1–3 and 2–4. In the case $J_1 = J_2$, the AF interaction is frustrated since then the cluster becomes tetrahedral. The effect of the s–ph interaction is not important for the IR with $S > 0$; thus, we shall only focus our attention on the spin-zero, A_1 and B_1 IR, both associated with the GS. Table 2 shows the explicit form of the eigenfunctions associated with the GS; the eigenstates of the spin operator $S_{z\ell}$ are represented by $\uparrow_\ell$ $(+\frac{1}{2})$ and $\downarrow_\ell$ $(-\frac{1}{2})$ respectively.

Table 2. The $S = 0$ eigenfunctions of H_s.

Notation	Eigenfunction
$\|A_1, S = 0\rangle$	$-\frac{1}{2}(\uparrow_1\downarrow_3 - \downarrow_1\uparrow_3)(\uparrow_2\downarrow_4 - \downarrow_2\uparrow_4)$
$\|B_1, S = 0\rangle$	$\frac{1}{\sqrt{12}}[2(\uparrow\downarrow\uparrow\downarrow + \downarrow\uparrow\downarrow\uparrow) - \uparrow\uparrow\downarrow\downarrow - \uparrow\downarrow\downarrow\uparrow - \downarrow\downarrow\uparrow\uparrow - \downarrow\uparrow\uparrow\downarrow]_{1234}$

In the case of a six-site ring, we perform a similar analysis; we first couple the spins $S_1 + S_3 + S_5 \equiv S'$ and $S_2 + S_4 + S_6 \equiv S''$, and then we couple S' and S'' to the total spin

Table 3. Separation of the Hilbert space of a six-site ring in terms of its IR. The sublattice and total spin are also shown.

S'	S''	S	Irreducible representation
$\frac{1}{2}$	$\frac{1}{2}$	0	$A_1 + B_1 + E_2$
$\frac{3}{2}$	$\frac{3}{2}$	0	A_1
$\frac{1}{2}$	$\frac{1}{2}$	1	$A_2 + B_2 + E_1$
$\frac{1}{2}$	$\frac{3}{2}$	1	$E_1 + E_2$
$\frac{3}{2}$	$\frac{3}{2}$	1	B_2
$\frac{1}{2}$	$\frac{3}{2}$	2	$E_1 + E_2$
$\frac{3}{2}$	$\frac{3}{2}$	2	A_1
$\frac{3}{2}$	$\frac{3}{2}$	3	B_2

S, separating the diverse resulting states in the IR of the geometric group C_{6v}. The results are summarized in table 3.

We have checked that the GS of the six-spin ring belongs to the bidimensional subspace $[A_1, S = 0]$ for the case $0 < 2J_2 < J_1$, or the one-dimensional subspace $[B_1, S = 0]$ for $2J_2 > J_1 > 0$. The s–ph interaction mixes these two IR subspaces. The GS is degenerate when $J_1 = 2J_2 > 0$, this being the condition for frustration of the AF interaction [22].

Table 4. The eigenfunctions associated with the GS of the six-ring expressed as resonant valence bonds. $K_1 = \sqrt{1/8}[\uparrow_1\downarrow_2 - \downarrow_1\uparrow_2][\uparrow_3\downarrow_4 - \downarrow_3\uparrow_4][\uparrow_5\downarrow_6 - \downarrow_5\uparrow_6] \equiv \check{b}_{12}\check{b}_{34}\check{b}_{56}$ and $K_2 = \check{b}_{23}\check{b}_{45}\check{b}_{61}$ are the traditional Kekulé bonding states, and $K_d = \check{b}_{14}\check{b}_{25}\check{b}_{36}$ represents bonding states along the diagonals of the hexagon. We remark that the states $|A_1, (\frac{1}{2})^2, S = 0\rangle$ and $|A_1, (\frac{3}{2})^2, S = 0\rangle$ are coupled by H_s.

Notation	Eigenfunction
$\|A_1, (\frac{1}{2})^2, S = 0\rangle$	$\sqrt{2}[K_1 + K_2 + 2K_d]/3$
$\|A_1, (\frac{3}{2})^2, S = 0\rangle$	$\sqrt{2}[K_1 + K_2 - K_d]/3$
$\|B_1, (\frac{1}{2})^2, S = 0\rangle$	$\sqrt{2/3}[K_1 - K_2]$

2.2. *The spin–phonon coupling*

The operator Λ defined in (3) belongs to the $[B_1, S = 0]$ IR of both C_{4v} and C_{6v} groups. Therefore H_{s-ph} mixes the IR $[A_1, S = 0]$ and $[B_1, S = 0]$, which compete for the GS of both $N = 4$ and $N = 6$ rings. On the other hand, the phonon operators a and $a^\dagger$, associated with the wavevector $k = \pi$, also belong to the $[B_1, S = 0]$ IR; accordingly, H_{s-ph} preserves the symmetry of the composite system of spins and phonons.

By using the results of tables 1–3 and analysing the effect of H_{s-ph} over the base vectors, we obtain the matricial expression for the Hamiltonian. In the case $N = 4$

$$H = [C + \omega(a^\dagger a + \tfrac{1}{2})]\mathbf{I} + \begin{bmatrix} \frac{1}{2}\Delta & -\sqrt{3}g\xi \\ -\sqrt{3}g\xi & -\frac{1}{2}\Delta \end{bmatrix} \tag{4}$$

where the basis for the spin part is ordered as $|A_1\rangle$, $|B_1\rangle$; $\xi = a + a^\dagger$ is the position operator of the lattice; $\mathbf{I}$ is the identity matrix; $C = -(2J_1 + J_2)$. Finally, $\Delta \equiv E_{A1} - E_{B1} = 4(J_1 - J_2)$. Thus, only the exchange difference $J_1 - J_2$ is relevant in the case $N = 4$.

In the case $N = 6$ we define $C \equiv -3(J_1 + J_2)$ and order the basis vectors as $|A_1, (\frac{1}{2})^2, S = 0\rangle$, $|A_1, (\frac{3}{2})^2, S = 0\rangle$ and $|B_1, (\frac{1}{2})^2, S = 0\rangle$, obtaining

$$H = [C + \omega(a^\dagger a + \tfrac{1}{2})]\mathbf{I} + \begin{bmatrix} 4J_1 & -2J_1 & -2g\xi \\ -2J_1 & -2J_1 + 6J_2 & -2g\xi \\ -2g\xi & -2g\xi & 0 \end{bmatrix}. \tag{5}$$

2.3. The adiabatic approximation

In order to obtain general insight into the system behaviour, it is useful to consider the adiabatic limit, where the ionic mass goes to infinity, or equivalently, $\omega \to 0$. Noting that the phonon momentum is $p = -\mathrm{i}(a - a^\dagger)/2$, since it fulfills the canonical commutation rule $[\xi, p] = \mathrm{i}$, we recast H_{ph} into the form $H_{\mathrm{ph}} = \omega(\xi^2/4 + p^2)$. In the adiabatic limit, the kinetic energy of the lattice is disregarded, and we can replace $H_{\mathrm{ph}} \approx \omega\xi^2/4$ in (1). Thus, the quantum position operator ξ becomes a classical variable. Rescaling the position variable $\xi \to X \equiv g\xi/2$, the Hamiltonian only depends upon J_1, J_2, X and $D \equiv 2g^2/N\omega$. Now the eigenenergies E_n, which depend parametrically on X, play the role of 'effective' (adiabatic) potentials for the ionic displacement, say $E_n = V_n(X)$. For example, in the case $N = 4$ the adiabatic potentials are

$$V_{(\pm)}(X) = C + \frac{1}{2D}X^2 \pm \tfrac{1}{2}\sqrt{\Delta^2 + 48X^2}. \tag{6}$$

Afterward, the ionic kinetic energy can be reinserted; the quantum status of the lattice displacements is then recovered in the context of the Born–Oppenheimer (BO) approximation. Introducing $M = N/(2g^2\omega)$ as an ionic mass, the BO Hamiltonian is

$$H_{\mathrm{BO},n} = H_{\mathrm{kin}} + V_n(X) = -\frac{1}{2M}\frac{\partial^2}{\partial X^2} + V_n(X). \tag{7}$$

To fix ideas, we return to the case $N = 4$. The adiabatic potential $V_{(+)}(X)$, associated with an excited state of H_s, has only one minimum located at $X = 0$. On the other hand, the GS adiabatic potential $V_{(-)}(X)$ has two possible behaviours. (i) $V_{(-)}(X)$ has a maximum at $X = 0$, and two symmetrical minima at positions $\pm X_{\mathrm{M}}$; for $|X| > X_{\mathrm{M}}$ the potential monotonically increases. In this case, a static distortion of the lattice is set up, giving rise to a spin-Peierls (SPD) phase. (ii) The potential $V_{(-)}(X)$ has a minimum at $X = 0$, increasing monotonically with $|X|$. In this case the adiabatic potential always leads to a 'softening' of the restoring force, but the system does not show SPD.

From (6) it follows that $D > D_{\mathrm{cr}} \equiv |\Delta|/24$ is the adiabatic condition for stabilizing the SPD phase. The amplitude of the distortion is given by $X_{\mathrm{M}} = \sqrt{12(D^2 - D_{\mathrm{cr}}^2)}$.

We have also analysed the lowest adiabatic potential of the six-ring; assuming AF couplings ($J_1, J_2 > 0$), this potential can only exhibit the two former behaviours: either it has two symmetric minima separated by a central maximum, or else it has one central minimum. If we move in the parameter space, the adiabatic potential *continuously* modifies its shape, and the system goes from the undistorted to the SPD state by suffering a *second-order phase transition*. This statement is true for both the four- and six-spin rings.

The last result, valid for AF couplings, contrasts with the ferro–antiferro Heisenberg model ($J_1 < 0$; $J_2 > 0$), where we have obtained *first-order Peierls transitions* between AF states of a six-ring, the latter one under the condition that $0.554\,605\ldots > J_2/|J_1| > \frac{1}{4}$ (the

last inequality assures that the GS is AF). The Hubbard model coupled with intramolecular phonons also exhibits first-order Peierls transitions [9, 11, 23].

Several calculations for the thermodynamic limit ($N \to \infty$) suggest that the 1D Heisenberg model is always dimerized, because the GS energy decreases with deformation as $X^{4/3}$, dominating over the X^2 law of elastic energy [10, 15].

If we consider a large enough phonon frequency ω, the adiabatic approximation is no longer reliable. In particular, if $D > D_{cr}$, but the phonon zero-point energy surpasses the adiabatic barrier, the SPD disappears, since then the lattice is not further trapped in a minimum of the adiabatic potential.

For very large lattice distortions our model becomes meaningless; in fact, we have assumed that the exchange interaction between sites ℓ and $\ell+1$, say $J_{\ell\ell+1}$, can be linearized with respect to lattice displacements; $J_{\ell\ell+1} = J_1 - g(u_{\ell+1} - u_\ell)$; here u_ℓ is the longitudinal movement of the ℓ ion. Since we are considering phonons with wavenumber $k = \pi$, it holds that $u_\ell = -(-1)^\ell X/(2g)$, and $J_{\ell\ell+1} = J_1 - X(-1)^\ell$. For ℓ odd, $J_{\ell\ell+1}$ decreases as X increases, vanishing as X attains the value $X = J_1 \equiv X_{max}$. A further increase in deformation $X_M > X_{max} = J_1$ should lead to an unphysical situation [7], since then the absolute value of $J_{\ell\ell+1}$ *increases with the interionic separation*. In order to exclude unphysical deformations, we impose

$$D < D_{max} \equiv \tfrac{1}{6}\sqrt{4J_1^2 - 2J_1J_2 + J_2^2}$$

in the case $N = 4$.

2.4. Evaluation of eigenfunctions

In the case $N = 4$, the eigenfunctions lying in the GS subspace, $[A_1, S = 0] \oplus [B_1, S = 0]$ have the form

$$|\Psi_E\rangle = \sum_{n=0}^{\infty} \sqrt{n!}[\alpha_n|A_1, S = 0\rangle + \beta_n|B_1, S = 0\rangle]|n\rangle \tag{8}$$

where $|n\rangle = \frac{1}{\sqrt{n!}}(a^\dagger)^n|0\rangle$ and $|0\rangle$ is the phonon vacuum. The coefficients α_n and β_n are determined from the eigenvalue equation $H|\Psi_E\rangle = E|\Psi_E\rangle$. Equation (4) yields the following tridiagonal system for the coefficients α_n:

$$\left(\frac{F_n - \Delta}{3g^2} - \frac{n}{F_{n-1}} - \frac{n+1}{F_{n+1}}\right)\alpha_n = \frac{\alpha_{n-2}}{F_{n-1}} + (n+1)(n+2)\frac{\alpha_{n+2}}{F_{n+1}} \tag{9}$$

where $F_n = E - J_2 + 4J_1 - \omega(n + \frac{1}{2})$. We note that each eigenfunction belongs to a fixed IR, say $[B_1, S = 0]$ or $[A_1, S = 0]$. (i) If Ψ_E belongs to the IR $[B_1, S = 0]$, equation (9) has the solutions $\alpha_{2n+1} = 0 = \beta_{2n}$. The GS corresponds to this case, as can be seen by taking the limit $g \to 0$. (ii) If Ψ_E belongs to the IR $[A_1, S = 0]$, then $\alpha_{2n} = 0 = \beta_{2n+1}$.

The set $\{\alpha_n\}$ is obtained by solving $Z_n \equiv \alpha_{n+2}/\alpha_n$ from the tridiagonal system (9). In the $n \to \infty$ limit, the physical solution must satisfy $\sqrt{n!}\alpha_n \to 0$, or equivalently $Z_n \sim 3(g/\omega n)^2$. By starting from a large enough n, and using the latter asymptotic relation, we obtain the Z_n in a decreasing sequence. We also evaluate the Z_n by starting from the left ($n = 0$ or $n = 1$) and compare both results at an intermediate value, $n = L$, thus obtaining the eigenenergy equation Z_L (left) = Z_L (right). In order to overcome numerical difficulties, L is chosen by imposing the condition that both iterative procedures, $Z_n \to Z_{n\pm1}$, must be stable (their Lyapunov exponents must be negative, say).

Once the set $\{\alpha_n\}$ has been evaluated for each eigenenergy, the eigenfunction (8) is obtained from the relations $F_n\beta_n = -\sqrt{3}g[(n+1)\alpha_{n+1} + \alpha_{n-1}]$.

The eigenvalue problem for the case $N = 6$ also leads to a tridiagonal equation, which is treated in a similar way.

2.5. Characterization of the spin-Peierls distortion

When an SPD is present, and therefore the adiabatic potential displays two minima, then one minimum corresponds to the 'static' configuration $[1 \leftrightarrow 2, 3 \leftrightarrow 4, \ldots]$ and the other one to $[N \leftrightarrow 1, 2 \leftrightarrow 3, \ldots]$. Due to QM effects, a tunnelling between these configurations exists. For a large ionic mass (or equivalently, small ω) the lower energy levels pair in narrow doublets. The tunnelling time between the two equivalent SPD is given by the inverse of the doublet width:

$$\mathcal{T} = \frac{2\pi}{E_1 - E_0}. \tag{10}$$

Here $\{E_j, j = 0, 1, 2, \ldots\}$ are the eigenvalues of the Hamiltonian (4). If $\mathcal{T}$ is very large in comparison to the lattice vibration time, $\mathcal{T} \gg 2\pi/\omega$, the distortion can be characterized as 'static'; otherwise the concept of an SPD is somewhat blurred.

3. Results

In this section we show some numerical results. We use $N = 4$, $J_1 = 0.25$ and $J_2 = 0$ unless otherwise specified. In fact, several conclusions are basically equivalent for the six- and four-spin clusters, but the latter case offers various closed expressions.

3.1. The energy levels

The adiabatic potential and exact eigenenergies for a distorted lattice ($D = 0.08$) are shown in figure 1(a) and (b). The cases of relatively small ($\omega = 0.05$) and moderate ($\omega = 0.15$) frequencies are considered. The lower energy levels appear as very narrow doublets for $\omega = 0.05$; these doublets split for the larger frequency.

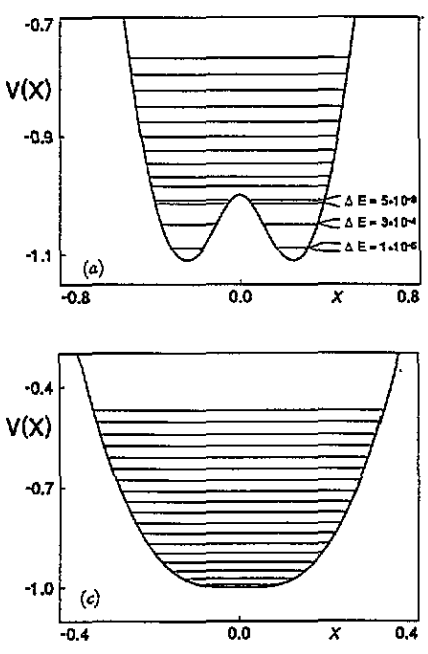

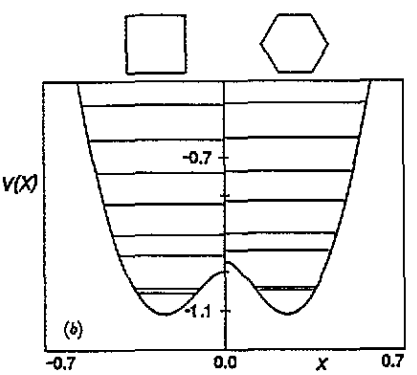

Figure 1. The ground-state adiabatic potential and the lower energy levels. The ring size is $N = 4$, except in the right-hand side of (b), where $N = 6$. The parameters are $\omega = 0.05$ in (a) and (c), and $\omega = 0.15$ in (b); $D = 0.08$ in (a) and (b) and $D = D_{cr} = 0.04\,166\ldots$ in (c). The doublet width is shown in (a).

In addition, figure 1(*b*) contrasts the adiabatic potentials and QM energy levels of a four-ring (left-hand side) and six-ring (right-hand side). In order to make a proper comparison of the two cases, we shift the energies in such a way as to make the adiabatic potential minima coincide, thus avoiding the effect of the superfluous additive constants. In spite of the fact that we are dealing with small rings, in which finite-size effects should be important, there is a relatively good accordance between the $N = 4$ and $N = 6$ cases. In particular, *the shapes of the adiabatic potentials coincide fairly well, while the energy levels are also* similar in both cases; for example, the zero-point energy $E_0 - V_{(-)}(X_M)$ is 0.056 and 0.061 for $N = 4$ and $N = 6$ respectively; however, the doublet width is slightly shorter in the latter case (0.011 and 0.0076 respectively), since then there is a higher adiabatic barrier (0.11 and 0.137 respectively).

Figure 1(*c*) shows the critical case, where the central barrier of $V_{(-)}(X)$ has just disappeared; we use $\omega = 0.05$. It is apparent that the lower levels show strong anharmonic effects, departing from the equidistant sequence of the harmonic case. This anharmonic behaviour can be understood from the BO approximation, since $[\partial^2 V_{(-)}/\partial X^2]_{X=0} = 0$ (here the accuracy of BO goes beyond the figure resolution).

Figure 2(*a*) shows $(E_j - E_0)/\omega$ against $g/\omega = \sqrt{2D/\omega}$ for $D = 0.06$. In particular, $(E_1 - E_0)/\omega$ nearly corresponds to the ratio between the vibration and tunnelling GS times; this ratio becomes very small for a highly dimerized system. The continuous curves are the exact QM results, while the dotted curves represent the BO calculations for $V_{(-)}(X)$. This adiabatic potential is fixed (since D is also fixed), and has a central barrier.

In the low-frequency regime, the barrier is nearly impenetrable, and the energy levels fuse in very narrow doublets; in addition, the QM and BO results virtually coincide, since the characteristic spin fluctuation time is very large in comparison with the vibration period. In the opposite limit of very large frequencies, the vibration amplitude is also large; therefore $V_{(-)}(X)$ can be approximated by the lattice contribution of (6), and the BO energy levels are roughly described by the relation $E_j = \omega(j + \frac{1}{2}) + \text{constant}$. On the other hand, the QM calculations closely follow the BO ones for low and moderate frequencies; in particular, the error in the GS doublet width is lower than 10% for $\omega \leqslant 0.3$, decreasing to 4% for $\omega \sim D$. An appreciable departure (over a 30% error) between BO and QM curves appears only for $\omega > 4(J_1 - J_2) = 1$, since then the energy levels of $V_{(-)}(X)$ overlap the upper adiabatic potential $V_{(+)}(X)$, thus causing strong non-adiabatic effects [12, 24].

It is very noticeable that the QM curves lie below the BO ones, as the latter implies *that the actual (QM) tunnelling time is larger than BO predictions, $\mathcal{T}_{QM} > \mathcal{T}_{BO}$. A similar* result was previously reported for the Peierls–Hubbard model [12]. This behaviour seems rather counterintuitive, since one should hope that the semiclassical character of the BO approximation must inhibit typical QM effects, such as quantum tunnelling.

Nevertheless, this surprising result can be understood in terms of a formalism [12, 24] in which the non-adiabatic effects are described by a gauge-field-like contribution. This non-adiabatic perturbation can be included approximately by modifying the adiabatic potential, $V_{(-)}(X) \to \overline{V}_-(X)$. *The central barrier becomes reinforced in $\overline{V}_-(X)$; accordingly, the* tunnelling time *increases* due to non-adiabatic effects.

This modified potential gives a very good account of the true QM results; for example, when $D = 0.06, \omega = 0.05$, the GS errors are -3×10^{-4} and 3×10^{-6} for the BO and modified potentials respectively; the departure from QM results has diminished by a factor of one hundred! The negative sign in the BO error is in accordance with the Brattsev theorem [25], which states that BO provides a *lower bound* for the GS energy. In addition, and for the same parameter values, the GS doublet width is overestimated by 4% and 0.4% by the BO and modified adiabatic potential respectively. The inequality $\mathcal{T}_{QM} > \mathcal{T}_{BO}$ can be

traced back to the reinforcement of the central barrier in the corrected potential, and the fact that $\overline{V}_-(X)$ closely reproduces the QM results.

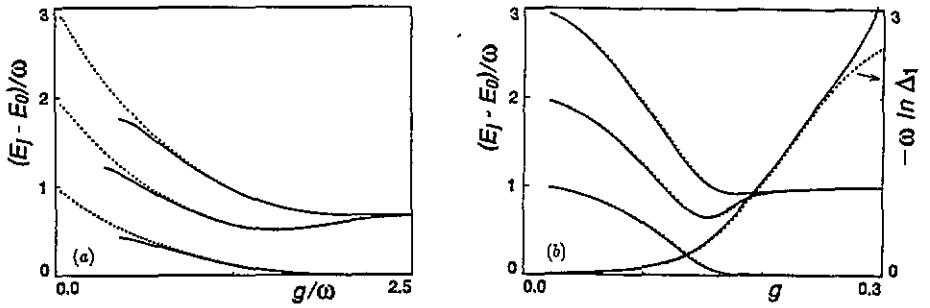

Figure 2. The excitation energies $E_j - E_0$, for $j = 1, 2, 3$. The BO calculations are shown by dots. In (*a*) $D = 0.06$. In (*b*), $\omega = 0.15$ and a plot of $-\omega \log[(E_1 - E_0)/\omega]$ is also shown.

A suitable measure of the degree of lattice dimerization is given by the rate $(E_2 - E_1)/(E_1 - E_0) = T/T_V$, where T_V can be associated with the 'corrected' lattice vibration time [12]. A remarkable result of figure 2(*a*) is the fact that the system is rather dimerized for relatively large frequencies ω. For example, in the case $\omega = 0.1$ (where the 'bare' zero-point energy is larger than the barrier height, $\omega/2 > V_M = 0.0336$) the following holds: $T/T_V \approx 3$. In spite of this relatively large T, the level E_1 is not trapped by the central barrier ($E_1 > V_{(-)}(X = 0)$, say); thus, the levels can pair in doublets, despite the fact that they eventually exceed the barrier top. To some extent this effect can be accounted for by the reinforcement of the central barrier of $\overline{V}_-(X)$ due to non-adiabatic corrections.

Figure 2(*b*) shows $(E_j - E_0)/\omega$ against g for a fixed frequency, $\omega = 0.15$. In contrast with figure 2(*a*), here $V_{(-)}(X)$ changes its shape with the s–ph coupling g (since D also changes). For a small g the adiabatic potential has a single minimum, and the lattice is undistorted; for a larger g two minima appear, separated by a central barrier which increases in size with g. The system develops an SPD when the GS becomes trapped by the barrier. As the barrier surpasses successive energy levels they fuse in doublets of decreasing width. Since $V_{(-)}(X)$ changes in shape as g increases, the doublet width shows a steeper narrowing in comparison to the case of figure 2(*a*).

In agreement with figure 2(*a*), the QM calculations yield a narrower GS doublet as compared to the BO case. To show in more detail the highly distorted region, where the GS doublet becomes exceedingly narrow, figure 2(*b*) also displays $-\omega \log(E_1 - E_0)$; that plot shows that the BO approximation becomes less accurate as the s–ph coupling increases for a fixed ω. The BO error is quadratic in g for small values of g, and linear for large values of this parameter. The error increases by over 10% when g surpasses $\omega (= 0.15)$.

From an analysis of the numerical results, we have concluded that, as $\omega \to 0$, the GS doublet width narrows according to $E_1 - E_0 \sim \omega \exp(-X_M\sqrt{2V_M/D\omega^2})$, where $V_M = V_{(-)}(0) - V_{(-)}(X_M)$ is the height of the central barrier.

Figure 3 shows a plot of the six QM lower energy levels of the IR B_1 in terms of the phonon frequency ω. For small ω, each level can be associated with a specific adiabatic potential, $V_{(+)}(X)$ or $V_{(-)}(X)$. However, when ω increases, such association becomes blurred since the BO approximation becomes less accurate. In particular, when two BO levels associated with different adiabatic potentials cross each other, the non-adiabatic corrections become particularly important; these non-adiabatic effects produce a 'repulsion' between the energy levels, precluding the crossing, in accordance with Teller's theorem.

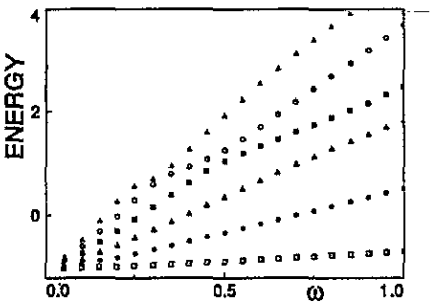

Figure 3. The six lower energies of the IR B_1 against ω for $D = 0.06$.

3.2. The lattice distortion

Let us consider the probability $P(\xi)$, where $\xi = a + a^\dagger = X/g$ is the lattice distortion. In the case of a dimerized lattice, $P(\xi)$ is a bimodal distribution with two symmetric maxima, $\pm\bar{\xi}$, associated with the dimerization amplitude; otherwise, $P(\xi)$ has a single maximum at $\xi = 0$. In the adiabatic limit $\bar{\xi} = \xi_M$. The value of $\mathcal{K} \equiv \langle\xi^4\rangle/[\langle\xi^2\rangle]^2$ is associated with the shape of $P(\xi)$ [11, 12]. In fact, on using the harmonic approximation to describe the minima of the adiabatic potential, we have

$$\langle\xi^2\rangle = \bar{\xi}^2 + \xi_0^2 \qquad \langle\xi^4\rangle = \bar{\xi}^4 + 6\bar{\xi}^2\xi_0^2 + 3\xi_0^4$$

where ξ_0 represents the mean square deviation of $P(\xi)$ around the maxima $\pm\bar{\xi}$. When a net dimerization exists, $\bar{\xi} \gg \xi_0$ and $\mathcal{K} \approx 1$. In the opposite limit, where the quantum fluctuations of ξ greatly exceed the dimerization amplitude, $\bar{\xi} \ll \xi_0$, then $\mathcal{K} \approx 3$; the tunnelling and vibration times are then comparable, and the notion of a dimerized state is no longer valid.

Figure 4(a) shows a plot of $\mathcal{K}$ against g for $\omega = 0.05$. Since the frequency is relatively small, the Peierls transition is sharp; $\mathcal{K}$ falls abruptly from three (undistorted lattice) to unity (SPD state) when g slightly crosses the critical value (associated with $D_{cr} = \Delta/24$), since then the $V_{(-)}(X)$ barrier appears. In contrast, for larger frequencies, the transition $\mathcal{K} = 3 \rightarrow 1$ becomes broad; it roughly occurs when the barrier height surpasses the 'bare' zero-point energy $\omega/2$.

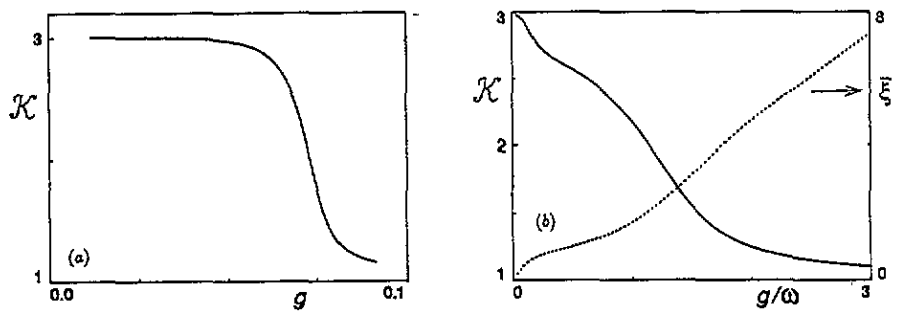

Figure 4. (a) The parameter $\mathcal{K}$ against g for $\omega = 0.05$. (b) The parameter $\mathcal{K}$ against g/ω for $D = 0.06$.

In figure 4(b) $\mathcal{K}$ is plotted against g/ω for $D = 0.06$. Thus, the adiabatic potential is now fixed, having two lateral minima. Accordingly, the variation of $\mathcal{K}$ is less steep than in figure 4(a). In addition, figure 4(b) shows the dimerization amplitude $\bar{\xi}$. For $g/\omega \rightarrow 0$, the

frequency goes to infinity, and the lattice is undistorted; say $\mathcal{K} \sim 3$, while $\overline{\xi} \sim 0$. As g/ω increases, ω and the energy levels E_n decrease (see figure 2(*a*)). The intermediate value $\mathcal{K} = 2$ is nearly attained when the first excited level E_1 descends below the barrier top, thus pairing in a doublet with the GS. The latter one occurs roughly when ω is three times larger than the barrier height; in spite of this fairly high frequency, there is an important degree of dimerization, since then $\overline{\xi} \sim 2.2$. For a further decrease in ω (right-hand side of figure 4(*b*)), the dimerization amplitude shows a steep increase, and $\mathcal{K} \to 1$.

3.3. Spin–spin correlation

Another measure of the degree of lattice dimerization is the second-neighbour spin–spin correlation

$$C_2 \equiv \frac{4}{N}\sum_{\ell=1}^{N}\langle S_\ell \cdot S_{\ell+2}\rangle.$$

This correlation attains its maximum value $C_2 = 1$ if the GS corresponds to $S' = S'' = N/2$; $S = 0$ (for example, this is the case of a rigid four-ring and $J_1 > J_2 > 0$). On the other hand, for a fully dimerized lattice, where correlation between second-neighbour spins is lost, it holds that $C_2 = 0$.

Since the total spin of the GS is zero, in the case of a four-ring the first- and second-neighbour spin–spin correlations are related by

$$2\langle S_\ell \cdot S_{\ell+1}\rangle = -\tfrac{3}{4} - \langle S_\ell \cdot S_{\ell+2}\rangle.$$

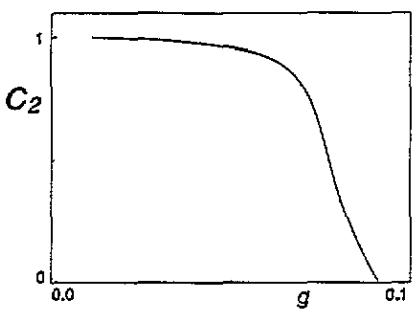

Figure 5. The spin correlation C_2 against g for $\omega = 0.05$.

Figure 5 confirms this discussion; in fact, there is a strong ferromagnetic second-neighbour correlation ($C_2 \sim 1$) for small and moderate values of g, in accordance with the antiferromagnetic (AF) character of the system. This correlation persists to $D = D_{cr} = 0.0415\ldots$, where $C_2 \approx 0.9$. For $D > D_{cr}$ the correlation C_2 shows a steep decrease as the SPD sets in, vanishing when D attains D_{max}; thereupon the model lacks physical meaning. For $D = D_{max}$ the system is fully dimerized.

3.4. Frustration and the spin-Peierls distortion

A cluster of four spins corresponds to a tetrahedron for $J_1 = J_2$. The AF interaction is then frustrated in the triangular faces, and the IR A_1 and B_1 of C_{4v} (associated with the GS) fuse in the bidimensional IR 'E' of T_d (see [21]). In such a case the tunnelling time $\mathcal{T} = 2\pi/(E_1 - E_0)$ becomes infinite due to degeneracy. In the BO approximation, $\mathcal{T}$ remains

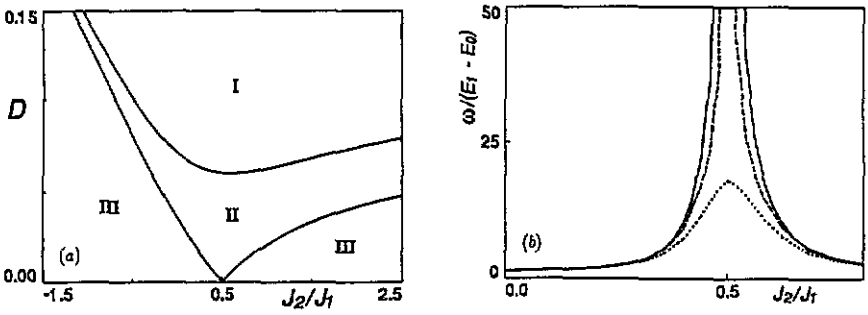

Figure 6. The case of a six-ring. (*a*) The phase diagram in the adiabatic limit. (*b*) A plot of $\omega/(E_1 - E_0)$ against J_2/J_1 for $J_1 = 0.25$, $D = 0.01\,667$ and $\omega = 0.05$.

finite (but very large) at $J_1 = J_2$; in that case $D_{cr} = 0$, and the height of the adiabatic barrier is maximal.

In the generic case of a $2N$ Heisenberg ring of spin-$\frac{1}{2}$ with first- and second-neighbour interactions, the frustration condition for $N > 2$ is $J_2 = \frac{1}{2}J_1$ (see [22, 26]). In order to attain this general case of frustration, we have studied a six-site ring. The results are shown in figure 6.

Figure 6(a) shows the phase diagram for the adiabatic limit. The upper-right part of the plane corresponds to the region of unphysically large distortions. The SPD phase occurs when the system parameters lie in the region II, while the undistorted phase corresponds to region III. In this way, for fixed J_2/J_1 our finite ring displays an SPD on increasing D; nevertheless, at the frustration condition $J_2/J_1 = \frac{1}{2}$ a *vanishing value of D is enough to yield a distorted state.* This behaviour is due to the fact that a frustrated state corresponds to a maximum of the spin energy, as the condition of AF correlations cannot be fulfilled for all neighbours; the latter one under the proviso that the lattice topology is unchanged. However, the system can depart (to some extent) from the frustration condition by means of dimerization, thus lowering its internal energy, even for a negligible s–ph coupling. In addition, the frustrated state is degenerate, and each wavefunction corresponds to neighbouring spins paired in singlets, thus producing a fully dimerized lattice [22]; therefore, the Peierls state can be assimilated to a Jahn–Teller distortion, in which the lattice accommodates to the (low-symmetry) spin wavefunction, regardless of the magnitude of the s–ph coupling.

Figure 6(*b*) shows $\omega/(E_1 - E_0) \sim \mathcal{T}/\mathcal{T}_V$ against J_2/J_1 for $J_1 = 0.25$, $D = 0.01\,667$ and $\omega = 0.05$; this corresponds to a horizontal line in the phase diagram of figure 6(*a*). The exact solution is represented by the full curve, while the dotted and broken curves correspond to the BO and modified-BO calculations respectively (the latter associated with the potential $\overline{V}_-(X)$). Figures 6(*a*) and (*b*) are in good accordance, as the tunnelling time is appreciably larger than $\mathcal{T}_V$ only in the distorted (II) region. This figure confirms that SPD is strongly enhanced by frustration, as the tunnelling time goes to infinity in the neighbourhood of the 'static' frustration condition, $J_1 = 2J_2$.

We define the 'dynamical' frustration condition by imposing $\mathcal{T} = \infty$, or equivalently a degenerate GS (for example, the lower energies of the IR A_1, $S = 0$ and B_1, $S = 0$ must coincide). According to our exact (QM) calculations, frustration occurs at $J_2/J_1 \approx 0.49\,968$ for the parameters of figure 6(*b*); for the same value of D and $\omega = 0.15$, frustration occurs at $J_2/J_1 \approx 0.49\,912$ yielding a deviation nearly linear in ω.

The BO calculation always leads to a finite tunnelling time, although a prominent peak appears at the frustration condition (note that vertical axis must be magnified by a factor

of 1000). On the other hand, the modified-BO calculation yields an infinite $\mathcal{T}$ when the frustration condition is fulfilled; this result occurs because the two lower adiabatic potentials intersect at $X = 0$, and therefore the non-adiabatic correction diverges at this point [12]. Thus the BO approximation is not too accurate in the neighbourhood of frustration; the modified-BO and the exact results are in good accordance, except in a narrow vicinity around the frustration point.

4. Summary and conclusion

The effect of lattice dynamics on a Peierls–Heisenberg system was studied by analysing rings of four and six spins. Exact quantum mechanical (QM) and Born–Oppenheimer (BO) calculations were carried out; a modified version of the BO approach [12] was also tested. The exchange spin–spin interaction was retained up to second neighbours. Only one vibrational degree of freedom was kept: that with wavevector $k = \pi$.

In general terms we have concluded that, for a large enough s–ph coupling g, the reciprocal influences between the spin and lattice degrees of freedom can be considerable. In fact, on comparing with an uncoupled system, a great distortion appears in the phonon levels, together with a substantial change in the spin–spin correlations. Our main results are outlined in what follows.

(i) For a small phonon frequency (where BO is suitable), our finite clusters exhibit a spin-Peierls distortion (SPD) if the s–ph coupling exceeds a critical value. For a four-spin ring this condition is $D > D_{cr} = |J_1 - J_2|/6$. Figure 6($a$) shows D_{cr} for the six-spin ring. If $D > D_{cr}$, the lower adiabatic potential $V_{(-)}(X)$ has two minima, and each minimum can be associated with one particular static SPD (say, $[1 \leftrightarrow 2, 3 \leftrightarrow 4, \ldots]$ or $[N \leftrightarrow 1, 2 \leftrightarrow 3, \ldots]$).

(ii) In the case of a non-vanishing frequency, QM effects produce a tunnelling between the two SPD states in a characteristic time $\mathcal{T}$, which decreases as ω increases. If $\mathcal{T}$ is large, the system behaviour is basically equivalent to a static distortion. But if $\mathcal{T}$ is comparable to the lattice vibration time, the image of an SPD state becomes blurred. In the low-frequency limit, $\mathcal{T}$ increases exponentially with $1/\omega^2$. The amplitude of an SPD also decreases as ω increases.

In analogy with conventional Peierls distortion [6], it is plausible that the tunnelling time becomes infinite for $N \to \infty$ and zero temperature. But for non-zero temperature the coherence length of SPD is finite, and therefore tunnelling must exist, even in the thermodynamic limit.

(iii) A small central barrier in the adiabatic potential may be enough to stabilize an SPD. In other words, relatively high frequencies are compatible with SPD; for example, for $\omega \approx 2V_M$, tunnelling times as large as 5.5 lattice vibrations appear.

(iv) In the AF Peierls–Heisenberg model only *second-order phase transitions* are allowed, as the lower adiabatic potential $V_{(-)}(X)$ has only one minimum at $X = 0$, or else two symmetric minima at $X = \pm X_M$, separated by a central barrier. In contrast, in the (frustrated) case of ferro–antiferro couplings, first-order Peierls transitions are possible.

(v) The SPD state is strongly enhanced in the neighbourhood of the frustrated regime. When the frustration condition is fulfilled *a 'static' dimerization* appears ($\mathcal{T} = \infty$).

In the case of a four-spin ring, the frustration condition is $J_1 = J_2$, regardless of the value of s–ph coupling or phonon frequency. But in the more generic case of a six-spin ring, the 'static' frustration condition ($J_1 = 2J_2$) is slightly modified for a non-vanishing ω (e.g., for a frequency as large as $\omega = 0.6J_1$ and $D = 0.067J_1$, the departure from this condition is lower than 0.2%).

(vi) BO calculations give a small error, even for relatively high frequencies; this is particularly true for the ground state. But BO fails when two levels associated with different adiabatic potentials nearly coincide, or else for unphysically large frequencies. We remark that the present work goes beyond a mere freezing of lattice coordinates at the minima of the adiabatic potential as we are performing a Born–Oppenheimer calculation, which reintroduces *a posteriori* the QM status of lattice variables [19].

Nevertheless, BO overestimates the tunnelling effect, *giving a shorter tunnelling time than actual QM results*, $\mathcal{T}_{BO} < \mathcal{T}_{QM}$, where $\mathcal{T}$ is the lifetime of a static SPD. The latter result is very surprising, as tunnelling is a typical QM effect; nevertheless, it can be understood in terms of some 'non-adiabatic gauge field' [12,24], which reinforces the central barrier of the BO potential.

Acknowledgments

This work has been supported by Fondecyt (project 1940341), DTI of the Universidad de Chile, and DICYT of the Universidad de Santiago. One of us (CE) is indebted to CONICYT for a Doctorate Grant scholarship.

References

[1] Gagliano E, Proetto C and Balseiro C 1987 *Phys. Rev.* B **36** 2257
[2] Baranowski D, Büttner H and Voig J 1993 *Phys. Rev.* B **47** 15472
[3] Zhang S C, Kivelson S and Goldhaber A S 1987 *Phys. Rev. Lett.* **58** 2134
[4] Sanyee Tang and Hirsch J E 1988 *Phys. Rev.* B **37** 9546
[5] Gottlieb D and Lagos M 1989 *Phys. Rev.* B **39** 2960
[6] Lee P A, Rice T and Anderson P W 1973 *Phys. Rev. Lett.* **31** 462
[7] Fradklin E and Hirsch J 1983 *Phys. Rev.* B **27** 1680 and references therein
[8] Hirsch J 1983 *Phys. Rev. Lett.* **51** 296
[9] Schmidt W and Schreiber M 1986 *Z. Phys.* B **62** 423
[10] Kuboki K and Fukuyama H 1987 *J. Phys. Soc. Japan* **56** 3126
[11] Proetto C and Falicov L 1989 *Phys. Rev.* B **39** 7545
[12] Cardenas M, Gottlieb D and Rössler J 1993 *Phys. Rev.* B **48** 10719
[13] Mahan G D 1986 *Many-Particle Physics* (New York: Plenum)
[14] Spalek J, Oleś A and Chao K 1981 *Phys. Status Solidi* b **108** 329
[15] Cross M C and Fisher D S 1979 *Phys. Rev.* **19** 402
[16] Werner H P, von Schütz J U, Wolf H C, Kremer R K, Gehrke M, Aumüller A, Erk P and Hünig S 1989 *Solid State Commun.* **69** 1127
[17] Visser R J, Oostra S, Vettier C and Voiron J 1983 *Phys. Rev.* B **28** 2074
[18] Jacobs S, Bray J W, Hart H R, Interrance L V, Kasper J S, Watkins G D, Prober D E and Bonner J C 1976 *Phys. Rev.* B **14** 3036
[19] Takahashi A 1992 *Phys. Rev.* B **46** 11550
[20] Hirsch J and Scalapino D J 1983 *Phys. Rev.* B **27** 7169; 1984 *Phys. Rev.* B **29** 5554
[21] Tinkham M 1964 *Group Theory and Quantum Mechanics* (New York: McGraw-Hill)
[22] Pimpinelli A 1991 *Phys. Rev.* B **43** 3710
[23] Takimoto J-I and Toyozawa Y 1983 *J. Phys. Soc. Japan* **52** 4331
[24] Rössler J, Esparza C and Toro A 1993 unpublished
[25] Epstein S 1966 *J. Chem. Phys.* **44** 836
Brattsev V S 1965 *Sov. Phys.–Dokl.* **10** 44
[26] Klein D J 1982 *J. Phys. A: Math. Gen.* **15** 661